MRS Communications (2015), 5, 97–114
© Materials Research Society, 2015
doi:10.1557/mrc.2015.18

MRS Communications

Polymers/Soft Matter Prospective Article

Bio-inspired responsive polymer pillar arrays

Elaine Lee and **Shu Yang,** Department of Materials Science and Engineering, University of Pennsylvania, 3231 Walnut Street, Philadelphia, Pennsylvania 19104, USA

Address all correspondence to Shu Yang at **shuyang@seas.upenn.edu**

(Received 8 March 2015; accepted 1 April 2015)

Abstract

High-aspect-ratio (HAR) pillar arrays offer large surface area, well-defined surface topography, and large mechanical compliance. In this Prospective, we showcase micro- and nanopillar array systems that exploit the responsiveness and/or harness the mechanical instabilities for myriad surface-mediated applications, including tunable wetting, adhesion, optical properties, and actuation. In each application, we start with biological examples with HAR pillar structures, and discuss strategies to fabricate responsive HAR polymer pillar structures. We then discuss approaches to tune the surface topography, such as via bending, tilting, expansion or contraction, and collapsing of the pillars, and the resulting change of surface and optical properties, and their dynamic actuation. In each system, we discuss the controllability and recoverability of pillar deformation.

Polymeric materials that are responsive to external stimuli, including temperature, pressure, pH, light, and electric and magnetic fields, are of interest for a wide variety of applications. Given the immense library of available constituents, the composition, functional groups, architecture, and multiscale morphology of polymeric materials can be tuned to induce dramatic and often reversible changes in shape,[1] volume,[2] morphology,[3] and mechanical[4] and optical properties.[5,6] By engineering the specific responsiveness, controlled transitions can be used for regulating wetting,[7] tunable adhesion,[8] expansion/contraction,[9] specific drug release,[10] and liquid passage through microfluidic channels.[1] Stimuli responsiveness arises from a system's ability to transition between two states of energy minima when triggered either physically (e.g., mechanically, electrically, magnetically, optically, and thermally), chemically (e.g., cross-linking, cycloaddition, zipping/unzipping, electrochemically, and ionically), or biologically.

Responsive polymers undergo conformational changes as a result of a change in the polymer chain interactions. Thermoresponsive polymers often possess either a lower or upper critical solution temperature, at which they undergo a coil-to-globule transition or vice versa.[11] A well-known example is poly(*N*-isopropylacrylamide) (PNIPAAm), which has a lower critical solution temperature (LCST) of ~32 °C. Above LCST, it becomes hydrophobic and collapses out of water. pH-responsive polymers have functional groups which are able to donate or accept protons under different pH conditions, which results in electrostatic repulsions between the resulting charges along the polymer backbone.[12] Polyacids, such as poly(acrylic acid) (PAA), release protons and swell at pH values above their pKa. Contrarily, polybases such as poly(vinyl pyridine) (PVP) accept protons and swell at pH values below their pKa. Optically responsive polymers are often achieved by the addition of photochromic molecules.[13] Common light-sensitive molecules include azobenzene, which undergoes a cis–trans isomerization; spiropyran, which ionizes and generates a dissociated ion pair; and cinnamate, which dimerizes and cross-links two molecules in response to UV irradiation.

While polymers readily respond to stimuli in solutions, polymers existing in other states of matter require greater energetic inputs for responsiveness due to their limited segmental motions, dimensional restrictions, and structural integrity. Common states of polymers include cross-linked gels, elastomers, and polymer solids. Stimuli-responsive gels are formed by chemically or physically cross-linking responsive polymers.[14] In particular, hydrophilic polymers can be cross-linked to form hydrogels that can swell in solvents, depending on temperature, pH, and ionic strength.[9–11] The responsiveness of hydrogels can be tuned by both the constituent polymers and their responsiveness, as well as by the cross-linking density and distribution of the hydrogels. Gels can be glassy in the dry state but exhibit a significant drop in modulus in the swollen state. Elastomers are polymer networks with low cross-linking density, allowing it to have high deformability and swelling in good solvents. Poly (dimethylsiloxane) (PDMS) is a typical elastomer that can be deformed mechanically due to its low elastic modulus, of the order of a few MPa.[15]

Liquid crystal elastomers (LCEs) are another unique class of elastomers, which combine the properties of liquid crystals (orientational order and responsiveness) and polymer networks (rubbery elasticity).[16] Like most elastomers, LCEs can exhibit either an isotropic random coil configuration or an anisotropic

https://doi.org/10.1557/mrc.2015.18 Published online by Cambridge University Press

stretched chain conformation, and the transition between these two phases can be triggered by a number of stimuli, including heat, light, solvent, and electrical field. Due to the permanent dipoles in the polymer matrices of LCEs and the resulting optical and geometrical anisotropies, LCEs can respond to electromagnetic fields by realigning their mean optical axis parallel to the external field, resulting in orientational changes.[17] In addition, the orientational order of the mesogens can be controlled by temperature or solvent as well as light with the addition of photochromic molecules,[18] resulting in conformation and/or shape change.[19] Since the strain in the polymer network is created by the anisotropic alignment of mesogens, LCEs exhibit a reversible shape memory effect, i.e., the permanent shape can be recovered upon removal of the stimulus or with the application of an additional stimulus.[18]

Glassy polymers or cross-linked networks typically have limited mobility and low free volume, resulting in restricted stimuli-responsive behaviors. To improve responsiveness, it is common to introduce a copolymer with a lower glass transition temperature (T_g) or add fillers to plasticize the polymer matrix and increase the free volume. Polymer networks can also be designed with cross-links, which can be reversibly broken upon triggering.[20] Polymers which can be programmed with a temporary shape and subsequently recover its permanent shape are known as shape memory polymers (SMPs).[21,22] Most commonly, the shape change is thermally induced, whereupon heating the SMP above a transition temperature (T_{trans}), typically the melting temperature (T_m) or the T_g, will decrease the Young's modulus by two or three orders of magnitude, allowing for the SMP to be deformed to a temporary shape. The temporary shape can then be fixed by fast cooling the sample. Reheating SMP in the temporary shape above T_{trans} triggers the relaxation of the stored elastic energy and the recovery of the permanent shape, which can be again fixed by quenching below T_{trans}. The process can be repeated to program a different temporary shape. Recent work has focused on the design of SMPs with multiple temporary shapes.[23–25]

To achieve multi-responsiveness, it is common to copolymerize different responsive monomers. It is also possible to embed responsive components within a polymer matrix to impose responsiveness. Typical responsive polymers and their chemical structures are summarized in Fig. 1. More extensive reviews of responsive polymers and their design and applications have been presented in literature.[26–28] In this review, we will focus on the design of geometrically defined surfaces, specifically micro- and nanopillar arrays from stimuli-responsive polymers or polymers with embedded responsive components for myriad of surface-related applications. Often, the properties of the materials are disproportionately dependent on the surface properties, including the chemistry and topography. While surface chemistry determines the intrinsic properties of the surface, surface topography (i.e., feature size, height, spacing, shape, and

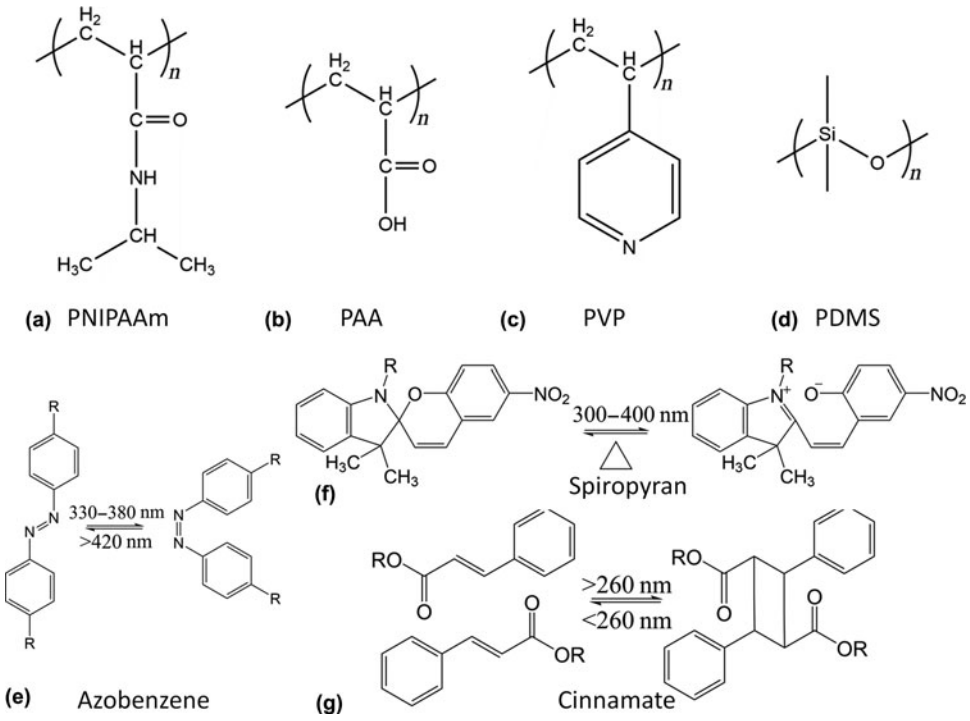


Figure 1. Chemical structures of common responsive polymers. (a) Thermo-responsive PNIPAAm, pH-responsive (b) PAA, and (c) PVP, (d) PDMS, and light-responsive (e) azobenzene, (f) spiropyran, and (g) cinnamate.

https://doi.org/10.1557/mrc.2015.18 Published online by Cambridge University Press

lattice symmetry) can be used to significantly alter the properties and add functionality. Inducing changes to the surface structure of polymeric materials results in a large change in its surface properties, including adhesion, wetting, optical appearance, and biocompatibility.[29–32]

In nature, there is an abundance of hierarchically patterns which offer multi-scale functionality and tunability, such as the self-cleaning and hydrophobic lotus leaves,[33–35] the chemically sensitive structural color of the "Morpho" butterfly wings,[36–38] and the adhesion pad of gecko lizards.[39–41] These properties arise from the micro- and nanostructures of the systems. Advances in micro- and nanofabrication techniques have allowed for the fabrication of multi-scale hierarchical structures with dynamic properties. Physical modification, through the combination of bottom-up self-assembly and top-down lithography techniques, is a simple and well-controlled approach to fabricate artificial multifunctional and well-ordered surfaces.[29–32] Biomimetic high-aspect-ratio (HAR) micro- and nanopillar arrays are topologically well-separated from the underlying substrate. Using responsive polymers to fabricate HAR pillar structures allows for the actuation of the patterned surface without changes to the bulk substrate, and leads to a variety of surface-mediated applications.[42] For some applications, it may be desirable to separate the active, responsive component from the bulk substrate. Often, responsive molecules or particles may be added to a polymer system. In this case, the polymer matrix provides the mechanical robustness/flexibility and the platform for actuation. In this Prospective, we present recent studies on responsive pillar arrays, showcasing their tunable behaviors and bio-inspired applications.

Tunable wettability

The lotus leaf is the quintessential example of a superhydrophobic surface in nature. The superhydrophobicity and self-cleaning properties of the lotus leaf are attributed to the array of microscale protrusions and the nanoscale roughness on the surface [Fig. 2(a)].[33–35] Decades of studies have shown that the roughness of a surface can dramatically affect its wetting properties, including apparent contact angle and contact angle hysteresis.[43–47] A superhydrophobic surface is characterized by a large water contact angle θ_w (>150°) with little contact angle hysteresis (typically less than 10°). When a water droplet sits atop a microstructure with air trapped between the droplet and the solid, a composite surface is formed. This surface can be described by the Cassie–Baxter model[48]:

$$\cos\theta^* = -1 + f_s(\cos\theta + 1), \quad (1)$$

where θ^* is the apparent contact angle of the composite surface, f_s is the area of the liquid–solid contact, and θ is the Young's contact angle on a flat surface of the same material.[48] When f_s becomes 1, i.e., the droplet is in contact with and wets the whole surface, the surface is described by the Wenzel model[49]:

$$\cos\theta^* = r\cos\theta, \quad (2)$$

where r is the surface roughness, i.e., the ratio of the actual to the apparent surface area.[48]

Another important factor to consider in the design of superhydrophobic surfaces is the contact angle hysteresis, i.e., the

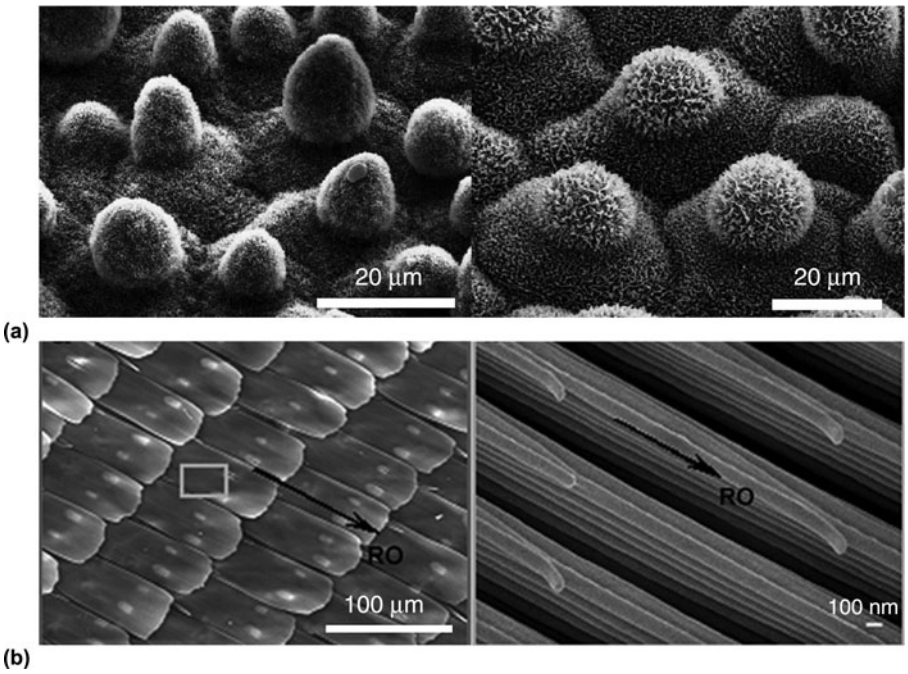


Figure 2. Hierarchical structures of the (a) lotus leaf[34] (Scale bars: 20 μm) and (b) butterfly wing (Scale bars: 100 μm and 100 nm).[53]

https://doi.org/10.1557/mrc.2015.18 Published online by Cambridge University Press

difference between the advancing (θ_a) and receding contact angles (θ_r). The contact angle hysteresis affects the droplet's adhesion to the surface and its ability to roll off with tilting. The sliding angle α, at which a droplet rolls off the surface, can be described by the Furmidge model[50]:

$$\sin\alpha = \frac{\sigma_{lv} w}{mg}(\cos\theta_r - \cos\theta_a), \quad (3)$$

where σ_{lv} is the surface tension of the water at the water–air interface, w is the width of the droplet, and m is the mass of the droplet. The "lotus effect" describes a superhydrophobic surface with low contact angle hysteresis and sliding angle, which results in easy roll-off of water particles and self-cleaning due to the low adhesion of water droplets. The "petal effect" describes a superhydrophobic surface with high contact angle hysteresis and high adhesive force.[51]

To mimic the superhydrophobic properties of natural systems, many studies have fabricated artificial substrates with controlled surface roughness. In particular, periodic micro- and nanopillar arrays were fabricated to mimic the surface protrusions of the lotus leaf. Additional functionalities assisted by superhydrophobicity can be found in these natural systems, including the self-cleaning of lotus leaves, paradoxical locomotion of water striders on water, and directional wetting of butterfly wings. Special wettability seen in nature is often correlated to multi-scale structured surfaces. As such, recent research has focused on the fabrication of hierarchically patterned surfaces which not only exhibit extremely large water contact angles, but have low contact angle hysteresis, possess robustness against impact pressure, mechanical rubbing, and extended exposure to outdoor conditions (e.g., sun, heat, and rain), dynamic tuning and directionality, and tunable adhesion.[31] Using responsive materials, the controlled deformation of surface structures can dynamically tune the surface roughness, and therefore the wetting properties.[52]

The *Morpho* butterfly wing exhibits directional non-wetting behavior, which arises from its hierarchical structure.[53] The wings are covered by overlapping micro-sized, periodically arranged rectangular scales, which align radially outward from the central axis of the butterfly body [Fig. 2(b)]. Each scale has nano-sized stripes which are oriented along the same direction as the scale. These stripes consist of multiple layers of cuticle lamellae of different lengths that are stacked stepwise along the microscales. Due to the anisotropy of this structure, water droplets can roll along but are pinned perpendicular to the direction of the nanostripes and microscales. Therefore, many groups have mimicked this structure by fabricating anisotropic micropillar structures, which are bent to induce directional wetting. Oblique electron beam irradiation,[54] ion beam irradiation,[55] and oblique metal deposition[56,57] have been used to fabricate tilted polymeric micropillars. By controlling both the surface chemistry and the tilting of the micropillars, the wetting of water droplets can be controlled to be pinned or propagated either uni-directionally or bi-directionally. However, the tilting of these pillars is not reversible.

For reversible and uni-directional wetting, a reconfigurable, water droplet-directing surface has been fabricated from HAR SMP pillars (Fig. 3).[58] The pillar dimensions are defined in Fig. 3(a). On the originally straight pillar array, water droplets are in the Cassie–Baxter state with a finite sliding angle. When heating the pillar array to a temperature above T_g, the pillars can be sheared to form uniformly deformed patterns and cooled below T_g to lock the structure [Figs. 3(a)–3(c)]. When the spacing of the pillars is smaller than the pillar height, the pillars can overlap with their neighbors to form saw-tooth-like structures [Fig. 3(c)]. On the deformed pattern, water droplets are in the Wenzel state and become fully pinned to the surface. Because the pillars are sheared in a specific direction, the wetting on tilted pillars is anisotropic, that is, the water contact angles are different in the direction along the tilting and perpendicular to the tilting. The water contact angle is lower along the direction of the deformed pillars [Fig. 3(d)]. This structure is analogous to one-dimensional wrinkled structures, which were previously shown to exhibit directional wetting.[59–61] The triple phase line is pinned along the channels because of the higher energy barrier in this direction [Figs. 3(e)–3(g)]. When the deformed pillars form a saw-tooth structure, the height variation adds additional roughness and increases the contact angle parallel to the deformed structure. Unlike previous studies, the deformed pillars can be recovered by reheating to above T_g. Exploiting this effect, a surface is designed with wettability contrast to direct water shedding from a region of straight pillars to one of deformed pillars [Fig. 3(h)]. This system allows for localized control of pillar deformation, and therefore localized wetting properties. By further exploiting these properties, an artificial water collection similar to that of the Namib Desert beetle can be envisioned.[62]

To locally control the heating of the SMP pillars, we recently reported the incorporation of gold nanorods (AuNRs).[63] Carbon nanotubes or nanofibers have previously been incorporated in the polymer matrix to reduce the thermal resistivity and increase the mechanical strength of SMPs for electroactive shape memory by resistive Joule heating. Incorporation of the AuNRs is not to improve the thermal conductivity. Instead, the AuNRs release heat when excited by a laser, while the conductivity of the SMP itself is low, allowing the local recovery of deformed SMP micropillars [Fig. 4(a)]. Light-responsive SMP micropillars (10 μm diameter, 40 μm height, and 20 μm pitch) were prepared by adding 0.1–0.2 mol% AuNRs. As prepared, the SMP micropillars were transparent and purple in color [Fig. 4(b); blue box]. The SMP pillars were bent at above the T_g to various angles depending on the applied force. When bent, the pillars become opaque [Fig. 4(b); red box]. As prepared, the static water contact angle of the SMP micropillars was about 160°. At a bending angle of 40°, the static water contact angle was reduced to 140°. When the pillars were fully collapsed, the contact angle further decreased to 100° [Fig. 4(c)]. The straight pillars, the high water contact angle, and

https://doi.org/10.1557/mrc.2015.18 Published online by Cambridge University Press

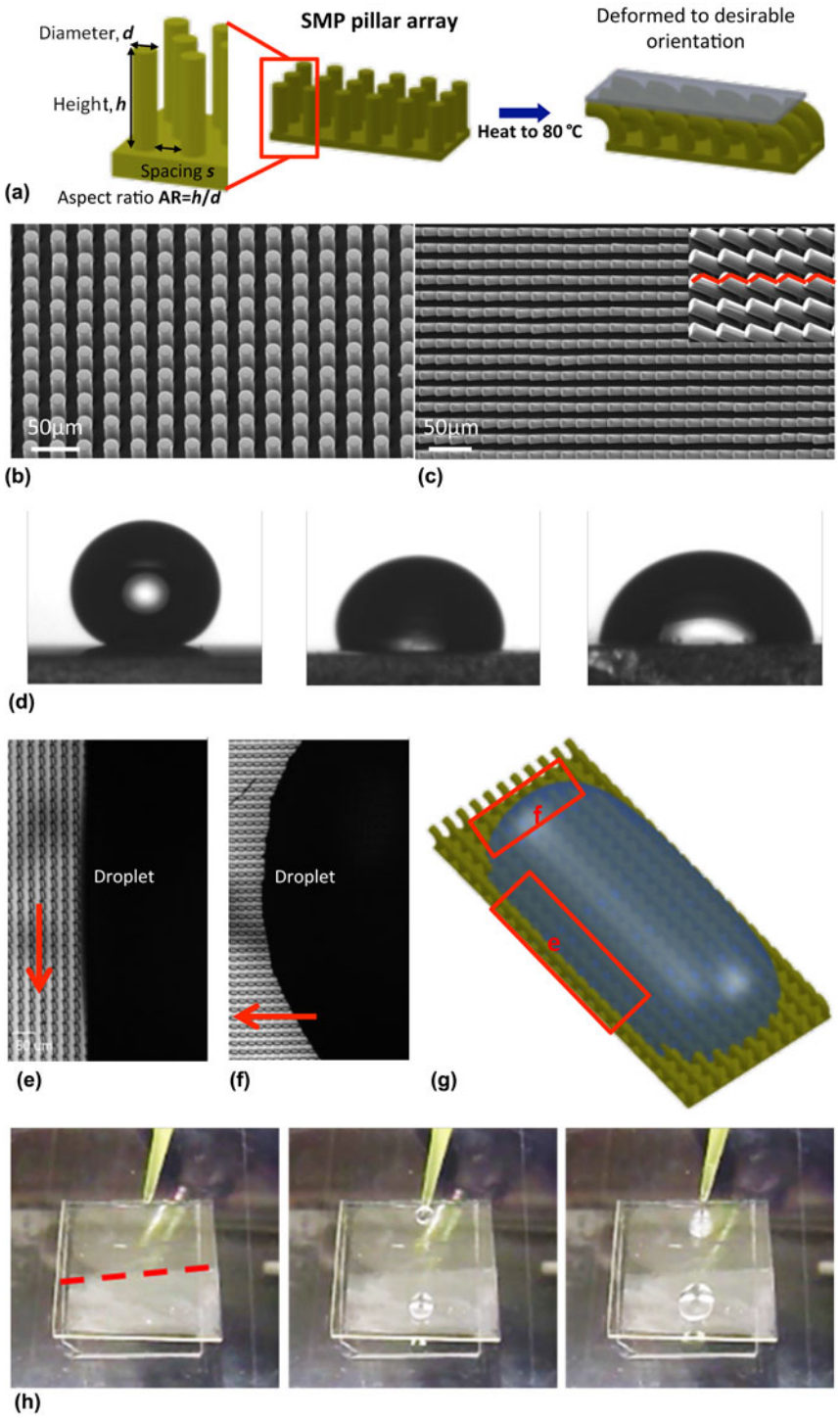


Figure 3. Design of water droplet-directing surface made of shape memory pillars. (a) Schematic presentation of the shearing of SMP pillars. (b, c) Scanning electron microscope (SEM) images of the original (b), and deformed (c) pillars. (d) From left to right: droplet viewed perpendicularly to the deformed pillars; water viewed in parallel to the deformed pillars; and the droplet on the original SMP pillars. (e) Triple phase line of water droplet on deformed pillars pinned along the deformed direction (red arrow). (f) Triple phase line of water droplet on deformed pillars unpinned perpendicular to the deformed direction (red arrow). (g) Schematic presentation of a droplet on deformed pillars, showing where the triple phase line is imaged in (e) and (f). (h) Wettability contrast between the original and deformed SMP pillar array. The sample stage is tilted by 10°. The upper half of SMP pillars are in the original state and the lower half is in the fully deformed state, as indicated by the dashed line.[58]

https://doi.org/10.1557/mrc.2015.18 Published online by Cambridge University Press

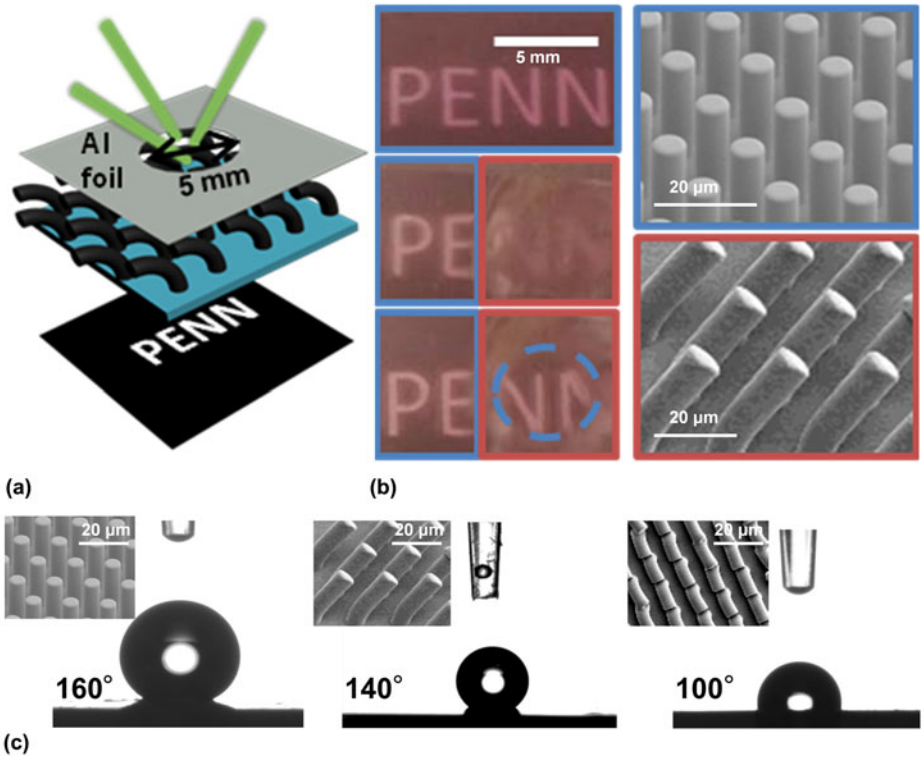


Figure 4. Design of light-responsive SMP micropillar arrays consisting of AuNRs. (a) Schematic presentation of the setup for local light exposure of SMP pillars. (b) Optical and SEM images of SMP–AuNRs at different stages. From top to bottom: pristine pillars; deformed pillars in the red box; recovered pillars within the dashed blue circle. (c) Water contact angles on various SMP–AuNRs micropillar arrays. From left to right: straight, partially bent (40°), and fully bent pillars.[63]

transparency can then be locally recovered by exposure to a green laser (wavelength 532 nm) through a mask for a few seconds [Fig. 4(b); dashed circle].

Another way to dynamically tune the contact area of the substrate with a droplet is by exploiting the anisotropy of nematic LCEs in micropillar arrays.[64] Because of the anisotropic alignment of the liquid crystal mesogens along the pillar axis, the pillars can reversibly contract (up to 70%) along the long axis and expand radially when heated to above the nematic to isotropic phase transition temperature (T_{NI}). Due to the change of surface topography, the contact angle of glycerol decreases from about 115° at 100 °C to about 80° at 140 °C [Fig. 5(a)] for pillars with diameter of 3 μm and height of 4 μm (D3H4). The area fraction of the surface contacted with the droplet, i.e., the diameter of the pillars, is increased by 12% upon heating to 140 °C. According to the Cassie–Baxter model, the theoretical contact angle is 140°, which is much higher than the measured value, suggesting that the glycerol drop is partially wetting the upper part of the pillar. Above the nematic to isotropic transition temperature, the contact angle of the pillars is similar to that of a flat surface of the same material, suggesting that the drop is in the completely wet Wenzel state. Upon cooling below the transition temperature, the pillars are reverted to their original dimensions but the liquid is trapped in the grooves, thus, the wetting transition cannot be reversed due to the high-energy barrier. With placing a new drop on the surface each time, the authors show that the contact angle can decrease and recover with repeated heating and cooling cycles, respectively [Fig. 5(b)]. The reversible tuning of wetting behaviors is achieved by the combination of the anisotropic LC alignment within the pillars, allowing for the expansion or contraction of the liquid/pillar contact area, and the pillar geometry [Fig. 5(c)].

Tunable adhesion

Gecko foot hairs have long been the fascinating natural model for dry adhesives due to their ability to quickly attach to and detach from a surface of almost any roughness or orientation without the use of liquid glue, bridge, or vacuum [Fig. 6(a)]. Each gecko foot pad consists of hundreds to thousands of hairs or setae arranged in lamellae [Fig. 6(b)]. Each seta [diameter ~5 μm, length ~30–130 μm; see Fig. 6(c)] branches out into hundreds to thousands of HAR fibrillar structures (diameter ~0.2–0.5 μm) known as spatulae [Fig. 6(d)]. High adhesion is achieved at a small pulling angle (α) between the millions of pre-sheared gecko spatulae and a surface [Fig. 6(e)] via van der Waals interactions[40] and possibly together with capillary forces.[65] At a high pulling angle, hairs can be detached [Fig. 6(f)]. To mimic this system, many groups have developed HAR pillar arrays to demonstrate dry adhesion, typically with

https://doi.org/10.1557/mrc.2015.18 Published online by Cambridge University Press

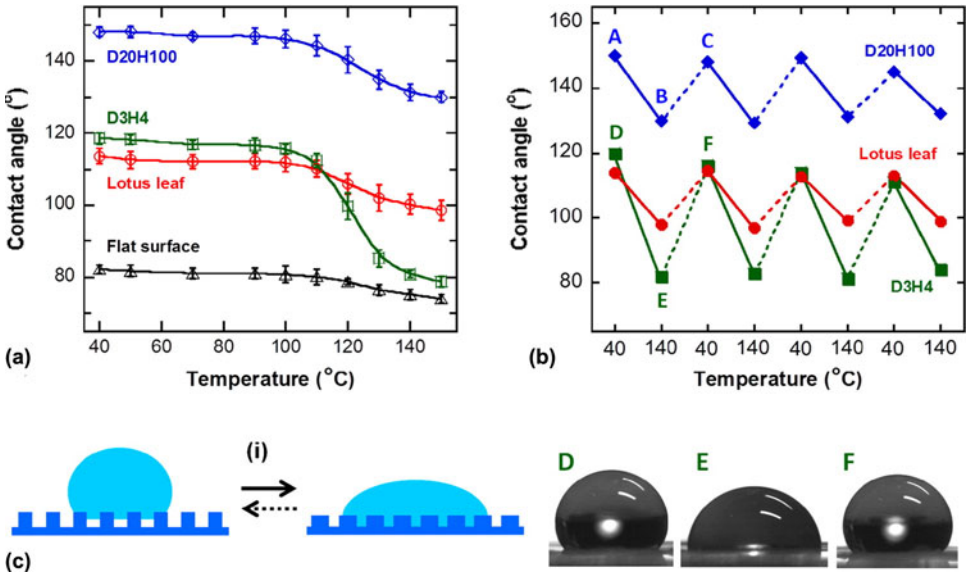


Figure 5. Design of dynamic wetting using LCE pillars. (a) Variation of contact angle of one glycerol drop on a responsive surface as a function of temperature during a continuous heating process. Flat LCE surface was used as the control. (b) Cyclic measurements of the glycerol contact angle for a structured surface switching between 40 and 140 °C. After each heating process, a new glycerol drop was put on a different place of the same surface at 40 °C. (c) Schemes describing the control of the wetting properties by tuning the roughness of surfaces covered with micropillars. Solid and dotted lines represent the temperature-induced change of wetting properties and the return to the original state using a new drop, respectively. The right images show the contact angles of glycerol on D3H4; D–F correspond to the points shown in panel (b).[64]

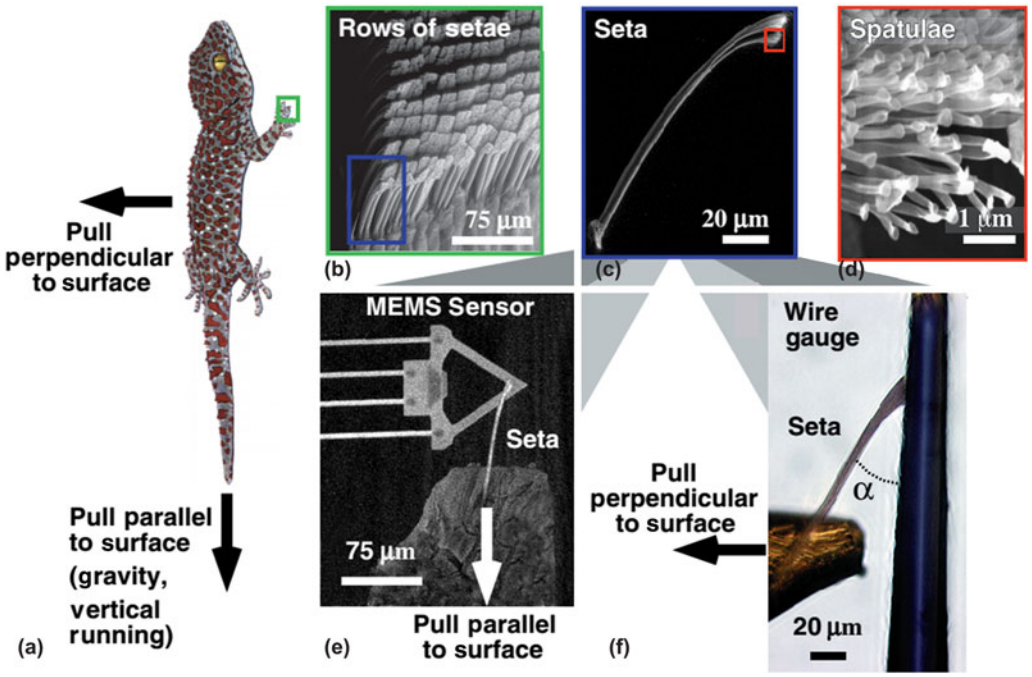


Figure 6. Structures of the gecko's foot hair and the experimental setup for measuring the adhesive force. (a) Tokay gecko (*Gekko gecko*) with toe outlined. (b–d) SEM images of (b) rows of setae from a toe, (c) a single seta, and (d) the finest terminal branches of a seta, called spatulae. (e) Single seta attached to a micro-electromechanical system (MEMS) cantilever capable of measuring force production during attachment parallel and perpendicular to the surface. (f) Single seta attached to an aluminum bonding wire capable of measuring force production during detachment perpendicular to the surface. α is the angle between setal stalk and wire gauge.[108]

https://doi.org/10.1557/mrc.2015.18 Published online by Cambridge University Press

adhesion strength of the order of a few N/cm^2.[55,56,66–68] To successfully mimic the gecko system, it is not only essential to achieve dry adhesion but also easy detachment. Therefore, the artificial pillar systems must also be responsive and reversible.

For example, a stretchable dry adhesive is fabricated with micropillars (20 μm in diameter, height, and spacing) atop microwrinkles with wavelength $\lambda = 80$ μm [Figs. 7(a) and 7(b)].[66] Here, the micropillars mimic the microstructure of the gecko foot, while the mechanical tilting of the pillars induces adhesion changes. By mechanically stretching the wrinkles made of elastomeric PDMS, the angle of the micropillar contact with a surface can be altered reversibly. Thus, the normal and shear adhesion of the substrate could be dynamically controlled. When the substrate is fully stretched and the wrinkles flattened, the micropillars are in the vertical position with maximal achievable contact. This results in a relatively high normal (~10.8 N/cm^2) and shear (~14.7 N/cm^2) adhesion. When the substrate is released, the micropillars are tilted and the contact area and resulting adhesion is drastically reduced. The substrate is shown to be durable for up to 100 cycles of attachment and detachment. This directionality dependence and reversibility is comparable with that of the gecko foot [Figs. 7(c) and 7(d)].

Alternatively, the shape memory effect of glassy polymers has been exploited to fabricate reversible, dry adhesives. By controlling the T_g, the applied pre-load, and the surface chemistry, strong reversible dry adhesion is demonstrated in epoxy-based SMP bulk films.[69,70] The release of the adhesive is achieved by macroscopically curving the samples at above the T_g[69] or by breaking the non-covalent hydrogen bonds

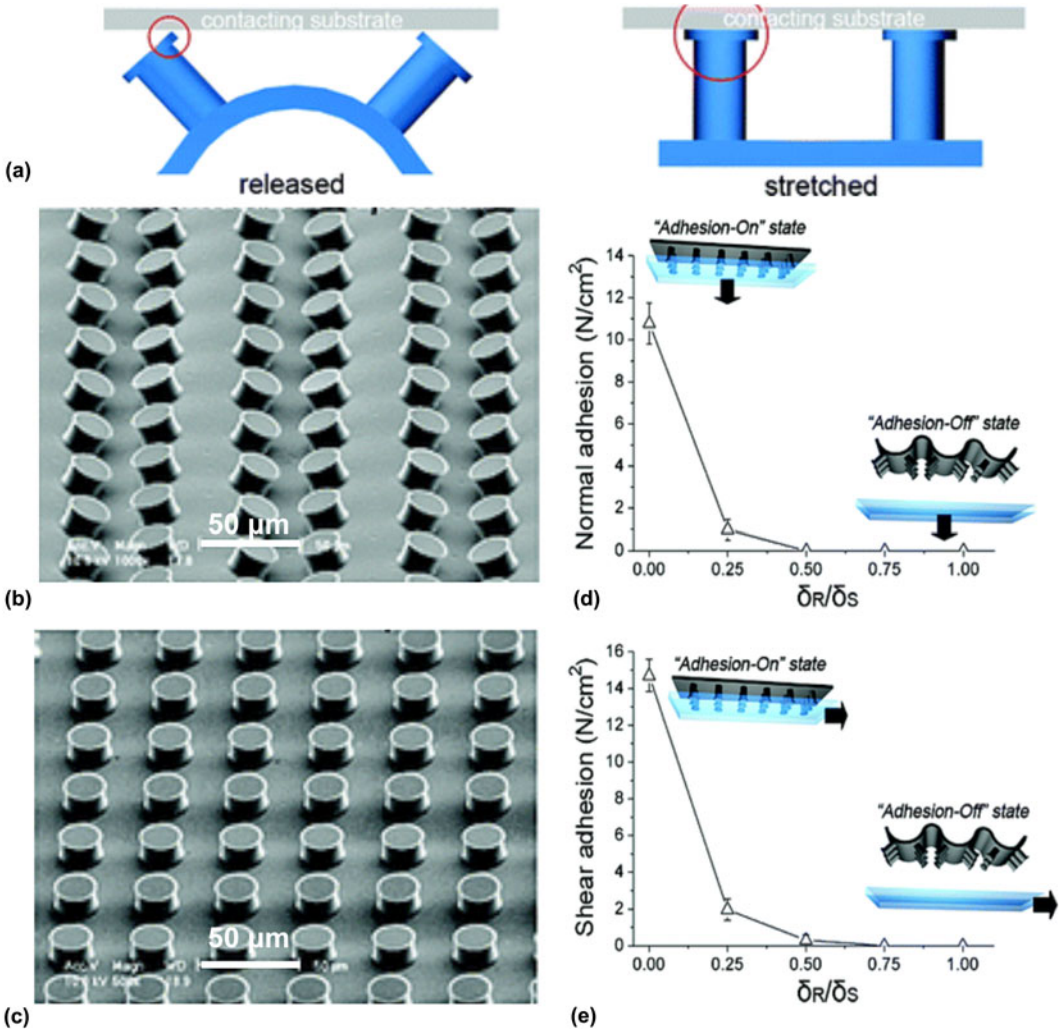


Figure 7. Design of reversible dry adhesive based on wrinkling of PDMS micropillars. Schematic presentation of the contact of the pillars with a flat substrate in the (a) released and strained states. SEM images of the (b) wrinkled and (c) as-prepared micropillars. Measurement of macroscopic normal (d) and shear (e) adhesion forces with a PDMS adhesive patch (thickness, 1 mm; size, 1 × 1 cm^2) having micropillars at different strain levels (δR/δS) against the smooth glass surface under a preload of 0.1 N/cm^2.[66]

https://doi.org/10.1557/mrc.2015.18 Published online by Cambridge University Press

between the two epoxy surfaces grafted with branched polyethyleneimine.[70] The latter is achieved through a peeling mechanism above T_g. The contact area of an SMP adhesive can be microscopically tuned by creating SMP micropillar arrays with controlled deformation [Fig. 8(a)],[68] Micropillars are used here due to their high mechanical compliance and deformability. As fabricated, SMP micropillar arrays [Fig. 8(b)] have relatively high adhesion with a pull-off force of about 30 kPa. The SMP is a cycloaliphatic polyetherurethane block copolymer phase-separated into two glassy domains with hard (T_g 120–140 °C) and soft segments (T_g 51 °C). The soft segments act as the shape memory switch, while the hard segments act as physical cross-linker to lock the deformed temporary shape. Upon heating to above the T_g of the soft segments (referred as T_{trans} in Fig. 8), the soft segments become flexible (storage modulus, E' changes from 1 GPa at 25 °C to 70 MPa at 70 °C). By applying a shear force, the SMP pillars can be tilted uni-directionally [Fig. 8(c)], switching the surface to a temporary non-adhering state with a negligible pull-off force. Upon reheating to above T_{trans}, the physical cross-links are unlocked, and the straight pillars [Fig. 8(d)] and adhesive state are recovered with a decreased pull-off force, ~12 kPa [Fig. 8(e)].

Velcro tape, based on the interlocking mechanism of hooks and loops of Burdock seeds,[71,72] is a quintessential example of a widely used reversible biomimetic dry adhesive [Figs. 9(a) and 9(b)]. Compared with gecko adhesion, which is of the order of a few N/cm^2, Velcro has achieved adhesion strength of ~120 N/cm^2.[73] Unlike the detachment of the gecko foot when pulled at an angle to the surface, more hooks and loops are engaged when Velcro is pulled parallel to its plane, resulting in higher adhesion strength. However, miniaturization of this mechanism has been difficult due to limitations in fabrication techniques to create hooks and loops in the micron scale. Instead, many recent studies have focused on enhanced dry adhesion between two surfaces with complementary structures, which exhibit anisotropic adhesion, i.e., large shear adhesion compared with normal adhesion.[74–83] In nature, interlocking surfaces can be found in the wings of beetles and the valves of diatoms with complementary structures [e.g., cones or triangles, see Figs. 9(c) and 9(d)].[82,84] Through the use of patterned structures, including random core–shell nanowires[76] and HAR polymer pillar arrays,[82] enhanced shear adhesion has been demonstrated due to the increased contact between complementary features. Pang et al. have recently demonstrated the use of anisotropic interlocking adhesion for pressure sensors.[81–83] Nevertheless, it is difficult to avoid buckling and collapsing of the pillars in any real applications, which is often considered detrimental to pillar–pillar contact at the interface, thus, lowering the adhesion strength.

By exploiting the shape memory effect and harnessing the buckling of HAR pillars, we show that both the normal and shear adhesion can be enhanced using complementary buckled SMP arrays made of diglycidyl ether of bisphenol A epoxy[74] through a combination of indentation and interweaving

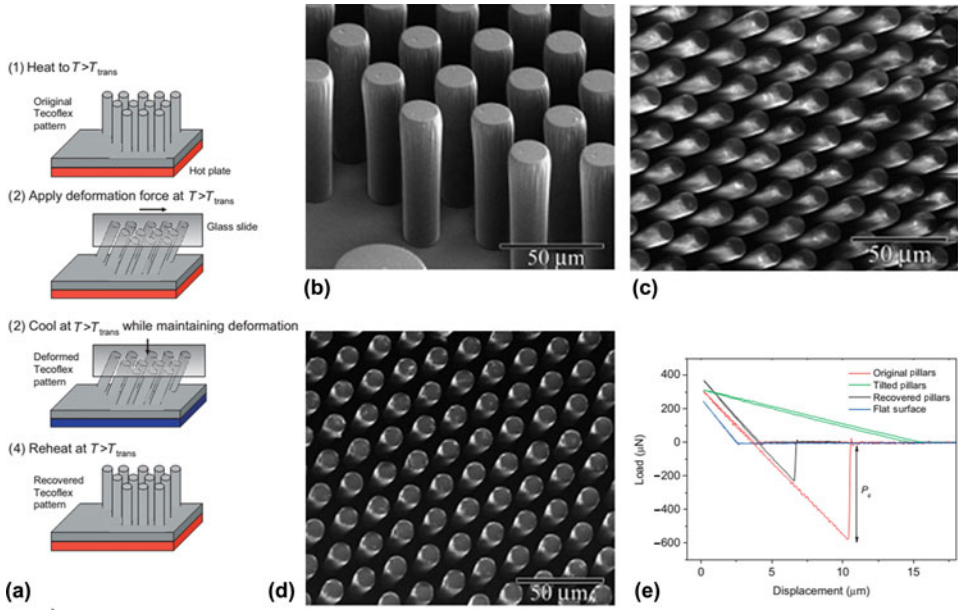


Figure 8. (a) The micropatterned surface is deformed by heating of the original Tecoflex surface with vertical pillars, followed by pulling of a glass slide over the top of the surface while the sample is at $T = 70$ °C. Cooling the system in the deformed position stabilizes the non-adhesive, tilted pattern. Recovery occurs by heating the pattern above its T_{trans}. SEM images of Tecoflex pillars with $r = 10$ μm, $h = 100$ and 20 μm interpillar spacing. (b) Original pattern. (c) Tilted pillars after deformation at 70 °C and fixation in the deformed state by cooling below T_{trans}. (d) Recovered pillars after reheating at 70 °C. (e) Load–displacement curves measured on the micropatterned surfaces.[68]

https://doi.org/10.1557/mrc.2015.18 Published online by Cambridge University Press

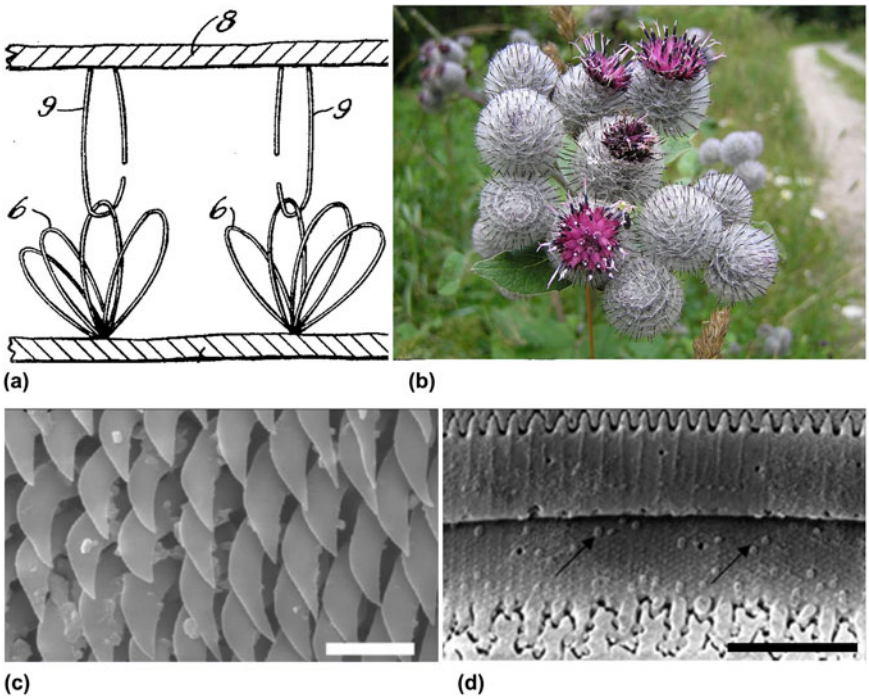


Figure 9. (a) Schematic illustration of Velcro.[71] (b) Photograph of a Burdock seed.[72] (c, d) SEM images of the (c) microstructure of microhairs on the surface of a beetle wing used for wing-locking[82] and (d) interlocking structure of valve structure of diatoms.[84] Scale bars, 5 μm.

mechanisms (Fig. 10). When two SMP pillar arrays are contacted at 80 °C (20 °C above T_g) with a preload larger than the critical buckling threshold, the pillars buckle and become indented and/or interweaved with each other [Fig. 10(a)]. The buckling behavior was confirmed by finite-element analysis [Fig. 10(b)]. The engaged structure is locked when the sample is cooled to room temperature, resulting in strong adhesion forces, ~53.6 ± 2.1 N/cm^2 in the normal direction and ~71.9 ± 23.2 N/cm^2 in the shear direction. These forces are much larger than those measured for non-interlocking SMP surfaces: pillar-to-flat (12.3 ± 8.8 N/cm^2, normal and 15.0 ± 2.3 N/cm^2, shear) and flat-to-flat contact surfaces (7.1 ± 5.0 N/cm^2, normal and 15.8 ± 2.0 N/cm^2, shear) [Fig. 10(c)]. The pillars can easily detach from each other when reheated to 80 °C. Using HAR micropillars, the contact area between the two complementary surfaces is significantly increased. In addition, the HAR of the pillars ensures that the critical aspect ratio for buckling is exceeded, allowing the SMP pillars to buckle against each other to maximize the contact area. While the normal and shear adhesion strengths are similar, the difference between them increases when the spacing ratio is increased. The overall adhesion also decreases with increasing spacing. Despite the significant increase of adhesion strength compared with the literature values (typically 10–20 N/cm^2 or less), buckling-based interlocking adhesives is for one-time use only. The indentation and/or interweaving of buckled pillars permanently deform the pillars, which cannot be completely recovered to the original straight configuration after reheating.

To enhance adhesion strength while not permanently deforming the pillars in contact, we embedded nanoparticles into the tips of elastomeric micropillars (Fig. 11).[77] The interactions between nanoparticles from the complementary pillars will provide the necessary interlocking mechanism, while the elastomeric nature of the pillars will allow for recovery of the deformed pillars, therefore reuse of the adhesive. Silica nanoparticles (diameter = 100 nm to 1 μm) were drop-cast over a PDMS mold (square array of cylindrical pillars with diameter = 5 μm) and bladed by a glass slide in one direction. UV-curable polyurethane acrylate precursor was then backfilled into the mold and photo-polymerized [Figs. 11(a) and 11(b)]. Two complementary surfaces can then be contacted and tested for shear adhesion strength [Fig. 11(c)]. The silica nanoparticles act as protrusions on the tip of the micropillars, which can be approximated as spatula-tipped pillars [Fig. 11(d)]. The composite pillar arrays have shear adhesion strength 48.5 N/cm^2, an order of magnitude higher than pristine pillar arrays (4.1 N/cm^2). The adhesion strength is found to be proportional to the particle size and the aspect ratio of the micropillars, and inversely proportional to the spacing ratio between the micropillars [Fig. 11(e)]. Similar to other systems with interlocking adhesion, particle-embedded pillars exhibit anisotropic adhesion strength, with their normal adhesion much lower than shear adhesion. However, since the pillars are elastomeric, two complementary surfaces can be detached in the normal direction without stripping the pillars from the supporting substrate. Therefore, the adhesive is reusable.

https://doi.org/10.1557/mrc.2015.18 Published online by Cambridge University Press

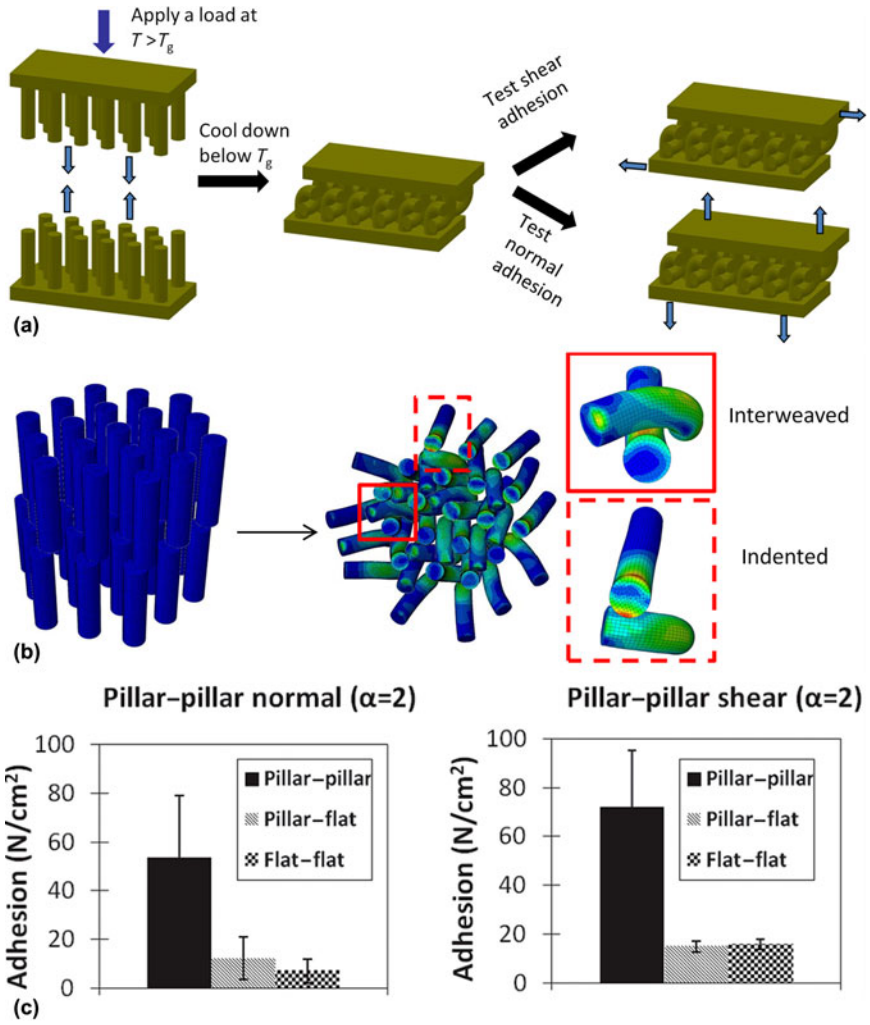


Figure 10. Design of interlocking adhesive system using SMP micropillars (diameter, 1 μm, aspect ratio, AR = height/diameter 4). (a) Schematic presentation of engaging pillar-to-pillar contact and adhesion measurement. (b) Finite element simulation of the contact process and collapse between two sets of pillars. (c) Measured adhesion strength from pillar-to-pillar, pillar-to-flat, and flat-to-flat contacts in the normal and shear directions. The spacing ratio = pillar-to-pillar distance/diameter, $\alpha = 2$.[74]

Tunable optical properties

Besides superhydrophobicity and directional wetting, butterfly wings are well known for their structural colors. Structural color results from the interference, diffraction, and scattering of light from micro- or nanostructures with lengths scales of the order of the wavelength of light. They are typically brighter and shinier than pigment colors, which could fade away over time under the sun. Structural color can be divided into two classes: angle-dependent color from coherent Bragg refraction on periodic structures, as seen in some of the butterfly wings and beetle scales,[85–87] and angle-independent color from quasi-amorphous structures, as seen in *Morpho* butterfly wings, bird feathers and mandrill skin.[88] While brilliant color is aesthetically pleasing, switchable color and/or transparency to suit the local environment may be desired in organisms for camouflage, signaling, or mating purposes.[89–91] For example, color changes are observed for *Morpho* butterfly wings in different vapors[37] [Fig. 12(a)] and longhorn beetle scales at different levels of humidity[91] due to changes of refractive index in the surrounding medium. Meanwhile, squids and octopi can switch between transparency and red color to become invisible to a predatory fish in down-welling light or to a predatory fish with bioluminescent searchlights, respectively, by stretching/contracting their skin to reveal/hide the pigments embedded within their chromatophores [Fig. 12(b)].[92,93] Previously, many groups have demonstrated the tuning of photonic crystals, which are characterized by periodically modulated refractive index, to switch between diffraction coloring and opaqueness in response to various stimuli.[94–97] However, such structures are unable to achieve transparency.

Chandra et al. have exploited capillary force induced clustering of polymeric micropillar arrays (diameter, 0.75–1 μm,

https://doi.org/10.1557/mrc.2015.18 Published online by Cambridge University Press

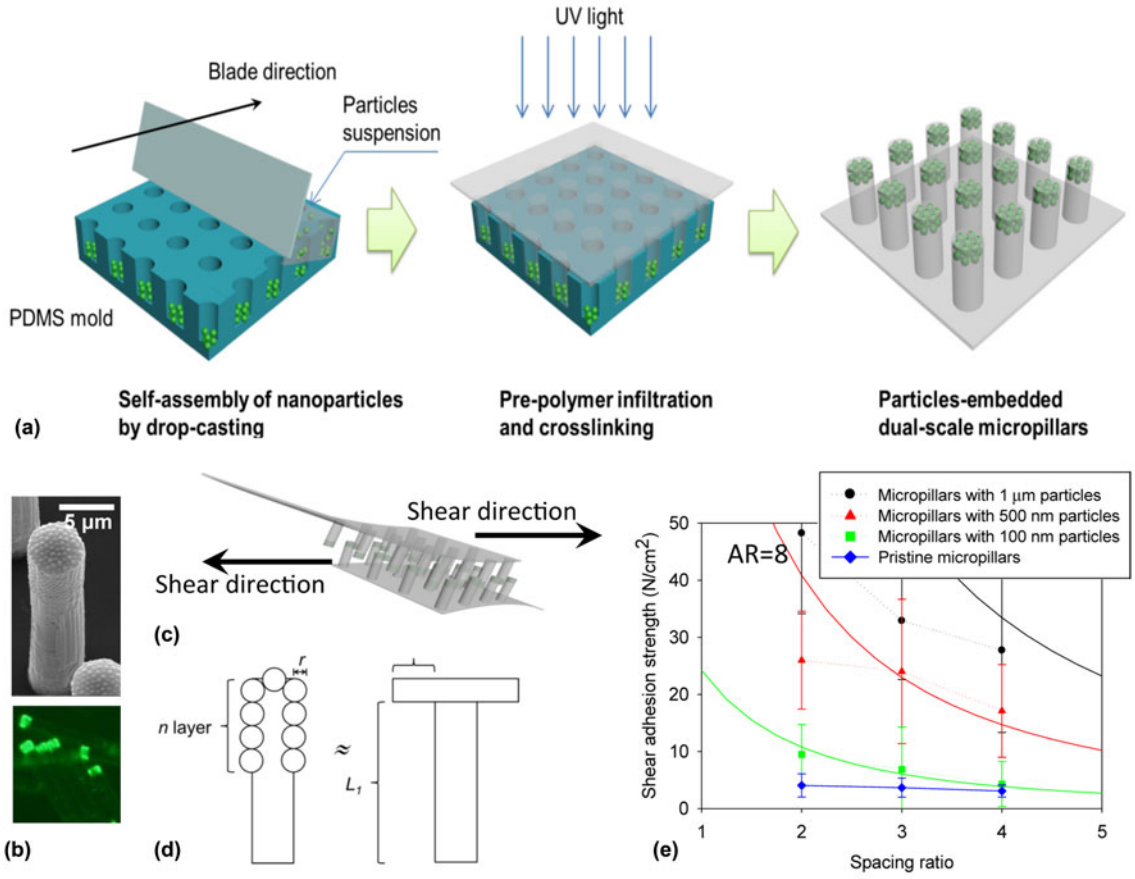


Figure 11. Design of interlocking adhesive system using micropillar arrays embedded with nanoparticles. (a–c) Schematic presentations of (a) the fabrication process, (b) the shearing of the interlocking pillars, and (c) a single pillar individual particle-embedded micropillar, approximated by spatula-tipped micropillar. (d) Top to bottom: SEM image of a particle-embedded micropillar; fluorescence image showing the distribution of silica nanoparticles at the tip of the micropillars. (e) Measured shear adhesion strength of smooth versus particles-embedded dual-scale micropillars (diameter, 5 μm) as a function of the spacing ratio. AR = 8.[77]

aspect ratio up to 12, pitch, 1.5–2 μm) and demonstrated switching from a colored film to ultrathin whiteness to transparency.[98] The unique optical properties are realized by a capillary-force-induced instability when drying poly(2-hydoxylmethacrylate-co-methyl methacrylate) (PHEMA-co-PMMA) micropillar arrays of different elastic modulus. The structural color arises from the Bragg diffraction from the straight, highly ordered pillars; the whiteness comes from the laterally collapsed, randomly arranged pillars; and the transparency from the ground collapsed pillars. However, the color of the original pattern is irrecoverable due to large van der Waals force between collapsed pillars. Lee et al.[7] have reported the reversible stretching of tapered PDMS nanopillar arrays (top diameter = 150 nm; bottom diameter = 300 nm; height = 150, 350, 700 nm) on a microwrinkled PDMS film (wavelength $\lambda = 31$ μm, amplitude $A = 4.4$ μm) for mechanically tunable wetting and transparency (Fig. 13). PDMS substrates pre-patterned with nanopillars were pre-stretched and treated with oxygen plasma to induce wrinkling [Fig. 13(a)]. As fabricated, the substrates are opaque but become transparent with strain [Figs. 13(b) and 13(c)]. The nanopillars render the substrates superhydrophobic. The switchable transmission (transparent ↔ opaque) is achieved primarily by reversibly flattening the microwrinkles, while the nanopillars are rather transparent in the visible wavelength.

We recently reported the reversible wrinkling of PDMS micropillars and demonstrated tuning between three states, from opaqueness to structural color display to transparency (Fig. 14).[99] Here, the surface-wrinkling effect is used to reversibly tilt PDMS micropillars. Due to the matching of the pillar (diameter = 1 μm, height = 4 μm, and spacing = 1 μm) and wrinkle dimensions (wavelength $\lambda = 2.4$ μm, and amplitude $A = 750$ nm), the wrinkle formation is confined by the micropillar array, which is different from the system by Lee et al.[7] Therefore, the pattern and wrinkle morphology, orientation and dimensions are controlled by varying the treatment duration of the oxygen plasma and the angle of uniaxial stretching with respect to the pillar array axis. While the original PDMS film exhibited angle-dependent colorful reflection due to Bragg diffraction

https://doi.org/10.1557/mrc.2015.18 Published online by Cambridge University Press

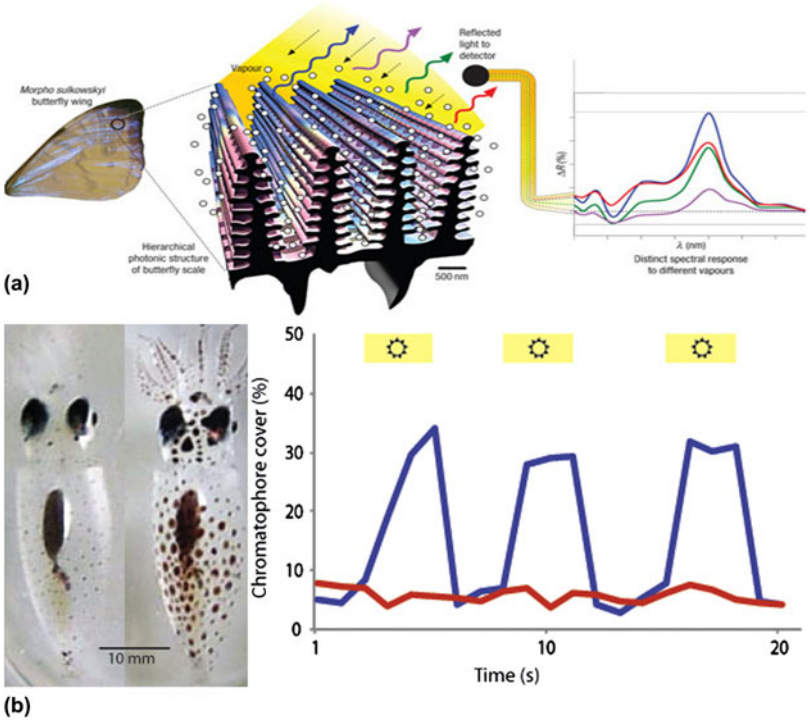


Figure 12. Dynamic coloring and transparency of biological systems. (a) Selective vapor response based on hierarchical photonic structures and demonstrated using *Morpho sulkowskyi* iridescent scales. Measurements of differential reflectance spectra ΔR provide information about the nature and concentration of the vapors: $\Delta R = 100\%$ times $(R/R_0 - 1)$, where R is a spectrum collected from scales upon vapor exposure and R_0 is a spectrum collected from scales upon exposure to a carrier gas (dry N_2).[37] (b) Left to right: Images of *Onychoteuthis banksii* showing the chromatophores contracted and the animal transparent under ambient light conditions; with the chromatophores expanded and the animal pigmented when subjected to directed light; optical responses of *O. banksii* to three bouts of directed light. The blue line indicates response to blue light, and the red line indicates response to red light. Yellow boxes with symbols show the onset and offset of each lighting bout. *O. banksii* stretches to expose chromatophores in response to blue light.[92]

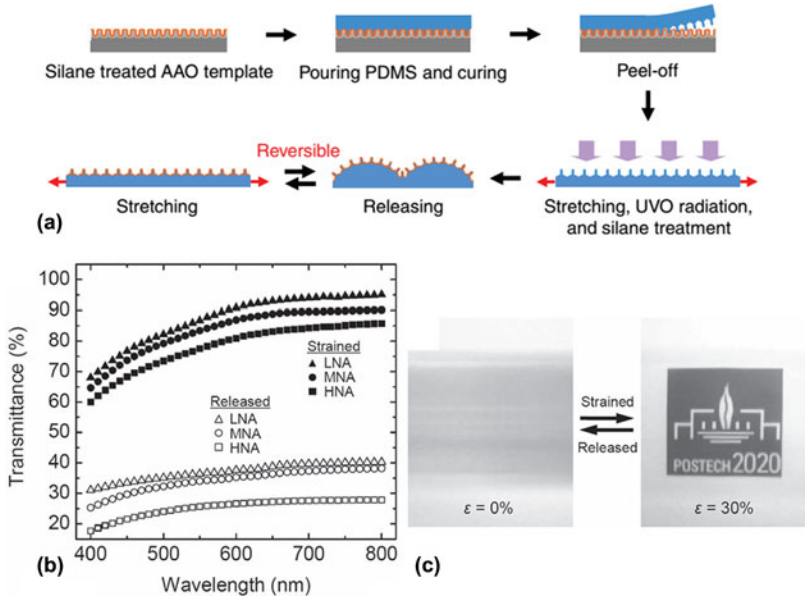


Figure 13. (a) Schematic illustration of the fabrication process of nanopillars (diameter, 150 nm) on microwrinkles (wavelength $\lambda = 31$ μm and amplitude $A = 4.4$ μm). (b) Transmittance spectra of the multi-scale structured PDMS films (with nanopillars of different aspect ratios) as a function of the mechanical state at normal incident light. (c) Optical images of the MNA film overlaying a printed paper.[7]

https://doi.org/10.1557/mrc.2015.18 Published online by Cambridge University Press

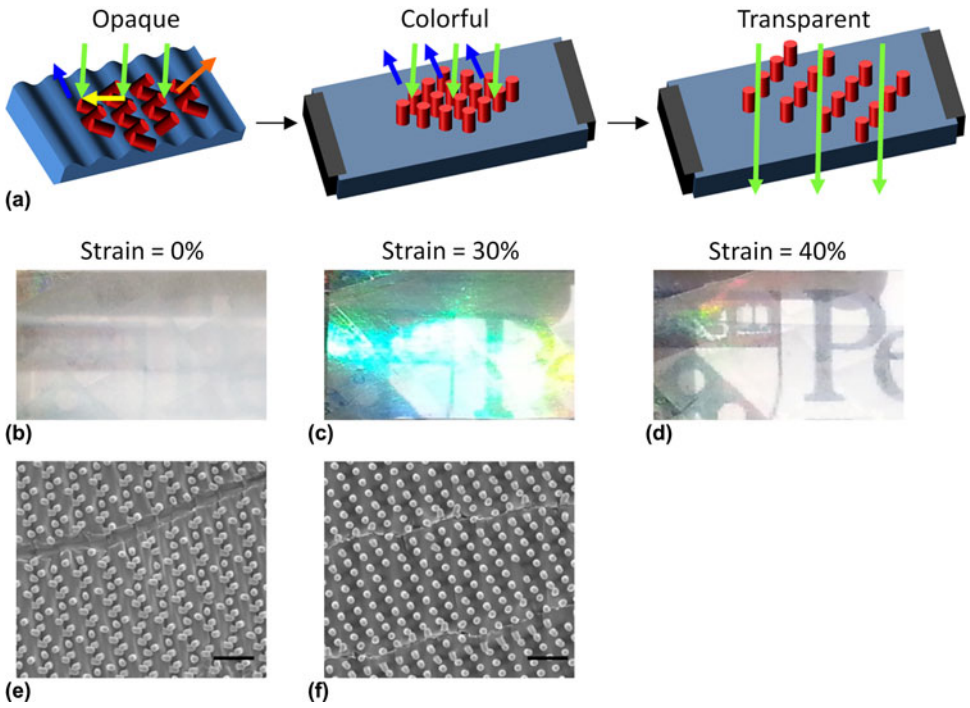


Figure 14. Tilted micropillars on wrinkled elastomers as a reversibly tunable optical window. Pillar diameter $D = 1$ μm, height $H = 4$ μm, and pitch $P = 2$ μm. The wrinkles have wavelength $\lambda = 2.4$ μm, and amplitude $A = 750$ nm. (a) From left to right: schematic illustrations of the tilted micropillar array after releasing the pre-strain, flattened micropillar array after re-stretching to 30%, and expanded pillar array after further stretching to 40%. Photographs of the substrate with incident light normal to the sample at (b) 0%, (c) 30%, and (d) 40% strain, and the corresponding SEM images for strains (e) 0% and (f) 30%. (e–f), Scale bars, 4 μm.[99]

of light from the periodic pillar array, the tilted pillar film appeared opaque. Upon re-stretching the film to the original pre-strain, the grating color is restored due to the straightened pillars and ~30% transmittance is recovered. Further stretching led to higher transmittance due to the increasing spacing between the pillars [Figs. 14(b)–14(f)]. The switch in optical properties is completely reversible over many cycles and is applicable for a cheap, controllable optical window. The reversible switch between color, transparency, and opacity is achieved by the micropillar array structure and the ability to reversibly actuate the orientation and spacing of the pillars.

Actuators

Mechanical actuation of HAR pillar structures is essential in natural systems for functions such as motion, self-cleaning, and food capture. For example, microorganisms use flagella for propulsion[100,101] and some respiratory tracts use cilia (diameter ~200 nm and length ~10 μm) for active anti-fouling

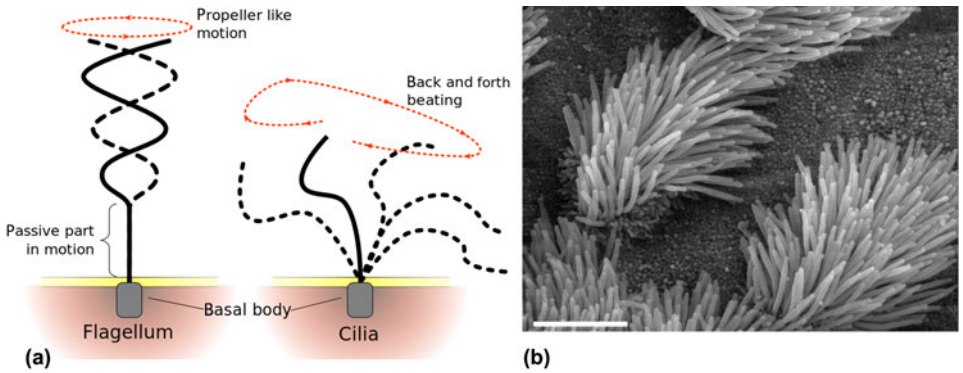


Figure 15. (a) Schematic presentation of flagellum and cilium motion.[101] (b) SEM micrograph of the cilia lining the respiratory epithelium in the lung (Scale bar: 5 μm).[102]

https://doi.org/10.1557/mrc.2015.18 Published online by Cambridge University Press

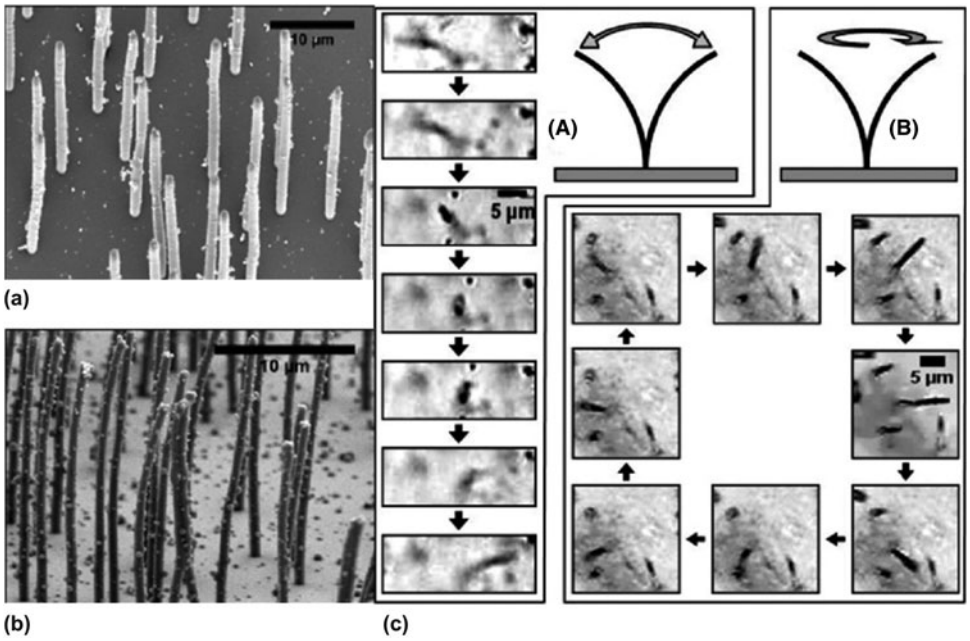


Figure 16. (a, b) SEM images of magnetically actuated PDMS pillar arrays embedded with Fe_2O_3 nanoparticles after being dried using supercritical CO_2. Pillar diameters, (a) 1 μm and (b) 700 nm. (c) Actuation of a single nanorod. (A) Linear and (B) rotational actuation strokes of a single 500 nm pillar with an aspect ratio of 50.[105]

(Fig. 15).[102–104] To mimic the motion of the cilia, HAR micro- and nanopillar arrays (diameter 100 nm–1 μm, AR up to 125) are fabricated from PDMS embedded with 18 wt% maghemite iron oxide (Fe_2O_3) nanoparticles [Fig. 16(a)].[105] In this case, the HAR and low modulus of the PDMS pillars lends its mechanical flexibility, while the nanoparticles are magnetic responsive. When actuated with an externally applied magnetic field, the pillars exhibit both linear and rotational responses, similar to that of biological cilia [Fig. 16(b)].

The responsive layer can also be separated from the pillar structures. HAR silicon nanopillars (diameters 100–300 nm, heights 5–8 mm, aspect ratios 15–80, and periodicities 2–4 μm) are embedded within a polyacrylamide gel (PAAG) grafted to a substrate [Figs. 17(a)–17(c)].[106] In this case, the hydrogel is the active, responsive layer while the stiff Si nanopillars provide the surface topography. The nanopillars can be tilted by the swelling or contraction of the hydrogel layer in response to humidity changes. Depending on the type of confinement of the Si nanopillars to the substrate, either non-touch [Fig. 17(d)] or directly attached [Fig. 17(e)], the nanopillars can be highly tilted or bent upon drying. Based on a similar concept, epoxy microfins (2 μm wide, 10 μm long, and 18 μm high) attached to a substrate are partially embedded in a pH-responsive hydrogel, poly(acrylamide-co-acrylic acid) or temperature-responsive PNIPAAm hydrogel layer, while the tips are stamped with catalysts or fluorescent dyes. The microfins can bend into and out of the reactant-containing layer actuated by the hydrogel layer, leading to repeated cycles of exothermic catalytic reactions synchronized with the mechanical motion of the microfins [Fig. 17(f)].[107] In this system, it is essential to have HAR pillars well separated from the reactant-containing liquid layer when inactive, as well as the underlying actuating hydrogel layer for maximal bending.

Conclusion

In this Prospective, we present recent literature on the bio-inspired design of responsive polymer pillar arrays with applications in tunable wetting, adhesion, optical properties and actuation. Biological systems achieve changes to their properties and functionalities by modulating their structures on multiple length scales. Inspired by nature, artificial HAR polymer pillar structures have been fabricated to engineer controlled and dynamic modifications to the surface topography, which can be triggered by a number of stimuli. Although many applications have been demonstrated at the laboratory scale, there are still limitations in applying polymer pillar systems at a commercial scale. Primarily, HAR pillars are prone to collapse due to mechanical instability. We envision the review presented here on existing strategies of fabrication and manipulation of HAR polymer pillars will shed light on applying HAR pillars to new paradigms, such as soft robotics and tissue engineering. Furthermore, by coupling with new innovations in patterning methods, such as three-dimensional printing, and combining bottom-up assembly and top-down lithography techniques, we expect researchers to create hierarchical structures with better programmability, controllability, and reusability on a large-scale to realize the maximum potential of responsive polymer pillar systems.

https://doi.org/10.1557/mrc.2015.18 Published online by Cambridge University Press

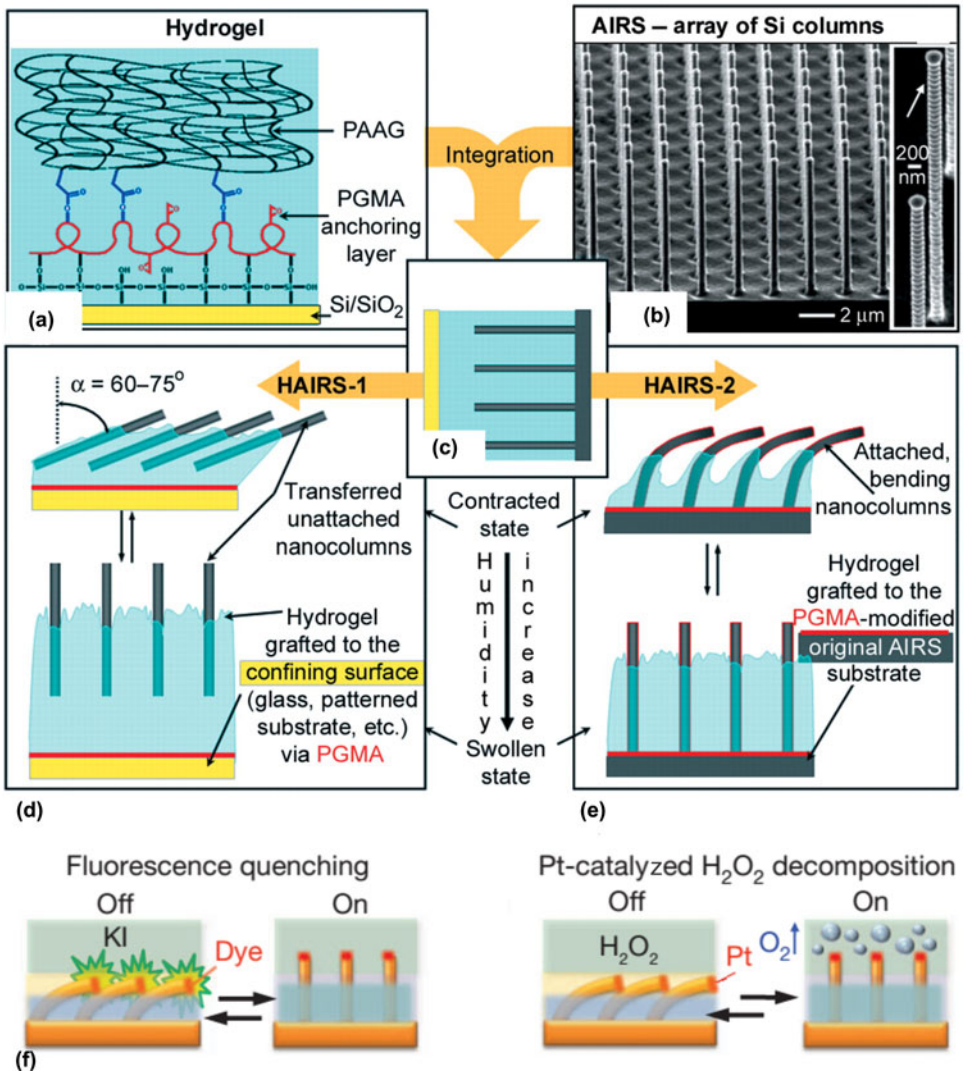


Figure 17. (a) Schematic presentation of the structure and composition of the PAAG film grafted to the Si/SiO_2 substrate via the polyglycidyl methacrylate (PGMA) anchoring layer. (b) SEM of a sample high AIRS composed of an array of silicon nanocolumns. (c) Hydrogel synthesis in the confinement of the AIRS and a secondary substrate. (d) Hybrid hydrogel-AIRS (HAIRS)-1 design. The nanocolumns, embedded into the hydrogel layer grafted to the PGMA-modified confining surface, break from the original wafer upon the separation of the confining substrates and become fully transferred onto the secondary surface. (e) Hybrid HAIRS-2 design. The hydrogel film is attached directly to the AIRS silicon wafer. Nanocolumns remain attached to the surface and bend upon drying.[106] (f) Schematic presentation of chemical reactions triggered by HAIRS bending. Left, fluorescent quenching. Right, platinum-catalyzed decomposition of hydrogen peroxide.[107]

Acknowledgments

The work shown here by the Yang laboratory was supported by the National Science Foundation (NSF) CAREER grant (no. DMR-0548070), GOALI grant (no. DMR-1105208), and EFRI-SEED grant (no. EFRI-1038215), and ACS/PRF grant (no. 50911-ND7).

References

1. T. Ohzono, H. Monobe, K. Shiokawa, M. Fujiwara, and Y. Shimizu: Shaping liquid on a micrometre scale using microwrinkles as deformable open channel capillaries. *Soft Matter* **5**, 4658 (2009).
2. K. Haraguchi, H.J. Li, L. Song, and K. Murata: Tunable optical and swelling/deswelling properties associated with control of the coil-to-globule transition of poly(N-isopropylacrylamide) in polymer-clay nanocomposite gels. *Macromolecules* **40**, 6973 (2007).
3. J. Kim, J. Yoon, and R.C. Hayward: Dynamic display of biomolecular patterns through an elastic creasing instability of stimuli-responsive hydrogels. *Nat. Mater.* **9**, 159 (2010).
4. K. Haraguchi and T. Takehisa: Nanocomposite hydrogels: a unique organic-inorganic network structure with extraordinary mechanical, optical, and swelling/de-swelling properties. *Adv. Mater.* **14**, 1120 (2002).
5. K.-U. Jeong, J.-H. Jang, C.Y. Koh, M.J. Graham, K.-Y. Jin, S.-J. Park, C. Nah, M.-H. Lee, S.Z.D. Cheng, and E.L. Thomas: Colour-tunable spiral photonic actuators. *J. Mater. Chem.* **19**, 1956 (2009).
6. C.H. Lee, H.S. Lim, J. Kim, and J.H. Cho: Counterion-induced reversibly switchable transparency in smart windows. *ACS Nano* **5**, 7397 (2011).

https://doi.org/10.1557/mrc.2015.18 Published online by Cambridge University Press

7. S.G. Lee, D.Y. Lee, H.S. Lim, D.H. Lee, S. Lee, and K. Cho: Switchable transparency and wetting of elastomeric smart windows. *Adv. Mater.* **22**, 5013 (2010).
8. P.-C. Lin, S. Vajpayee, A. Jagota, C.-Y. Hui, and S. Yang: Mechanically tunable dry adhesive from wrinkled elastomers. *Soft Matter* **4**, 1830 (2008).
9. L. Dong, A.K. Agarwal, D.J. Beebe, and H. Jiang: Adaptive liquid microlenses activated by stimuli-responsive hydrogels. *Nature* **442**, 551 (2006).
10. P. Gupta, K. Vermani, and S. Garg: Hydrogels: from controlled release to pH-responsive drug delivery. *Drug Discov. Today* **7**, 569 (2002).
11. D. Schmaljohann: Thermo-and pH-responsive polymers in drug delivery. *Adv. Drug Deliv. Rev.* **58**, 1655 (2006).
12. S. Dai, P. Ravi, and K.C. Tam: pH-responsive polymers: synthesis, properties and applications. *Soft Matter* **4**, 435 (2008).
13. Y. Zhao and T. Ikeda: *Smart Light-responsive Materials: Azobenzene-containing Polymers and Liquid Crystals* (John Wiley & Sons, Hoboken, New Jersey, 2009).
14. S.-k Ahn, R.M. Kasi, S.-C. Kim, N. Sharma, and Y. Zhou: Stimuli-responsive polymer gels. *Soft Matter* **4**, 1151 (2008).
15. J. Lötters, W. Olthuis, P. Veltink, and P. Bergveld: The mechanical properties of the rubber elastic polymer polydimethylsiloxane for sensor applications. *J. Micromech. Microeng.* **7**, 145 (1997).
16. M. Warner and E.M. Terentjev: *Liquid Crystal Elastomers* (Oxford University Press, New York, 2003).
17. C.M. Spillmann, B.R. Ratna, and J. Naciri: Anisotropic actuation in electroclinic liquid crystal elastomers. *Appl. Phys. Lett.* **90**, 021911 (2007).
18. I.A. Rousseau and P.T. Mather: Shape memory effect exhibited by smectic-C liquid crystalline elastomers. *J. Am. Chem. Soc.* **125**, 15300 (2003).
19. D.L. Thomsen, P. Keller, J. Naciri, R. Pink, H. Jeon, D. Shenoy, and B. R. Ratna: Liquid crystal elastomers with mechanical properties of a muscle. *Macromolecules* **34**, 5868 (2001).
20. C.J. Kloxin and C.N. Bowman: Covalent adaptable networks: smart, reconfigurable and responsive network systems. *Chem. Soc. Rev.* **42**, 7161 (2013).
21. A. Lendlein and S. Kelch: Shape-memory polymers. *Angew. Chem. Inter. Ed.* **41**, 2034 (2002).
22. P.T. Mather, X.F. Luo, and I.A. Rousseau: Shape memory polymer research. *Ann. Rev. Mater. Res.* **39**, 445 (2009).
23. T. Xie: Tunable polymer multi-shape memory effect. *Nature* **464**, 267 (2010).
24. I. Bellin, S. Kelch, R. Langer, and A. Lendlein: Polymeric triple-shape materials. *Proc. Natl. Acad. Sci. U. S. A.* **103**, 18043 (2006).
25. T. Xie, X. Xiao, and Y.T. Cheng: Revealing triple-shape memory effect by polymer bilayers. *Macromol. Rapid Commun.* **30**, 1823 (2009).
26. F. Liu and M.W. Urban: Recent advances and challenges in designing stimuli-responsive polymers. *Prog. Polym. Sci.* **35**, 3 (2010).
27. M.A.C. Stuart, W.T. Huck, J. Genzer, M. Müller, C. Ober, M. Stamm, G. B. Sukhorukov, I. Szleifer, V.V. Tsukruk, and M. Urban: Emerging applications of stimuli-responsive polymer materials. *Nat. Mater.* **9**, 101 (2010).
28. D. Roy, J.N. Cambre, and B.S. Sumerlin: Future perspectives and recent advances in stimuli-responsive materials. *Prog. Polym. Sci.* **35**, 278 (2010).
29. W.-G. Bae, H.N. Kim, D. Kim, S.-H. Park, H.E. Jeong, and K.-Y. Suh: 25th anniversary article: scalable multiscale patterned structures inspired by nature: the role of hierarchy. *Adv. Mater.* **26**, 675 (2014).
30. J. Zhang and Y. Han: Active and responsive polymer surfaces. *Chem. Soc. Rev.* **39**, 676 (2010).
31. M. Liu, S. Wang, and L. Jiang: Bioinspired multiscale surfaces with special wettability. *MRS Bull.* **38**, 375 (2013).
32. Z.B. Hu, Y.Y. Chen, C.J. Wang, Y.D. Zheng, and Y. Li: Polymer gels with engineered environmentally responsive surface patterns. *Nature* **393**, 149 (1998).
33. Y.T. Cheng, D. Rodak, C. Wong, and C. Hayden: Effects of micro-and nano-structures on the self-cleaning behaviour of lotus leaves. *Nanotechnology* **17**, 1359 (2006).
34. W. Barthlott and C. Neinhuis: Purity of the sacred lotus, or escape from contamination in biological surfaces. *Planta* **202**, 1 (1997).
35. C. Neinhuis and W. Barthlott: Characterization and distribution of water-repellent, self-cleaning plant surfaces. *Ann. Bot.* **79**, 667 (1997).
36. S. Kinoshita, S. Yoshioka, and K. Kawagoe: Mechanisms of structural colour in the Morpho butterfly: cooperation of regularity and irregularity in an iridescent scale. *Proc. R. Soc. Lond. B, Biol. Sci.* **269**, 1417 (2002).
37. R.A. Potyrailo, H. Ghiradella, A. Vertiatchikh, K. Dovidenko, J. R. Cournoyer, and E. Olson: Morpho butterfly wing scales demonstrate highly selective vapour response. *Nat. Photonics* **1**, 123 (2007).
38. P. Vukusic, J. Sambles, C. Lawrence, and R. Wootton: Quantified interference and diffraction in single Morpho butterfly scales. *Proc. R. Soc. Lond. B, Biol. Sci.* **266**, 1403 (1999).
39. H. Gao, X. Wang, H. Yao, S. Gorb, and E. Arzt: Mechanics of hierarchical adhesion structures of geckos. *Mech. Mater.* **37**, 275 (2005).
40. K. Autumn, M. Sitti, Y.A. Liang, A.M. Peattie, W.R. Hansen, S. Sponberg, T.W. Kenny, R. Fearing, J.N. Israelachvili, and R.J. Full: Evidence for van der Waals adhesion in gecko setae. *Proc. Natl. Acad. Sci. U. S. A.* **99**, 12252 (2002).
41. K. Autumn and A.M. Peattie: Mechanisms of adhesion in geckos. *Integr. Comp. Biol.* **42**, 1081 (2002).
42. D. Chandra and S. Yang: Stability of high-aspect-ratio micropillar arrays against adhesive and capillary forces. *Acc. Chem. Res.* **43**, 1080 (2010).
43. X. Zhang, F. Shi, J. Niu, Y.G. Jiang, and Z.Q. Wang: Superhydrophobic surfaces: from structural control to functional application. *J. Mater. Chem.* **18**, 621 (2008).
44. P. Roach, N.J. Shirtcliffe, and M.I. Newton: Progess in superhydrophobic surface development. *Soft Matter* **4**, 224 (2008).
45. D. Quéré: Wetting and roughness. *Annu. Rev. Mater. Res.* **38**, 71–99 (2008).
46. M. Miwa, A. Nakajima, A. Fujishima, K. Hashimoto, and T. Watanabe: Effects of the surface roughness on sliding angles of water droplets on superhydrophobic surfaces. *Langmuir* **16**, 5754 (2000).
47. X.J. Feng and L. Jiang: Design and creation of superwetting/antiwetting surfaces. *Adv. Mater.* **18**, 3063 (2006).
48. A.B.D. Cassie and S. Baxter: Wettability of porous surfaces. *Trans. Faraday Soc.* **40**, 546 (1944).
49. R.N. Wenzel: Resistance of solid surfaces to wetting by water. *Ind. Eng. Chem.* **28**, 988 (1936).
50. C.G. Furmidge: Studies at phase interfaces. I. the sliding of liquid drops on solid surfaces and a theory for spray retention. *J. Colloid Sci.* **17**, 309 (1962).
51. L. Feng, Y.A. Zhang, J.M. Xi, Y. Zhu, N. Wang, F. Xia, and L. Jiang: Petal effect: a superhydrophobic state with high adhesive force. *Langmuir* **24**, 4114 (2008).
52. B.W. Xin and J.C. Hao: Reversibly switchable wettability. *Chem. Soc. Rev.* **39**, 769 (2010).
53. Y. Zheng, X. Gao, and L. Jiang: Directional adhesion of superhydrophobic butterfly wings. *Soft Matter* **3**, 178 (2007).
54. T.-i Kim and K.Y. Suh: Unidirectional wetting and spreading on stooped polymer nanohairs. *Soft Matter* **5**, 4131 (2009).
55. Y. Rahmawan, T.-i Kim, S.J. Kim, K.-R. Lee, M.-W. Moon, and K.-Y. Suh: Surface energy tunable nanohairy dry adhesive by broad ion beam irradiation. *Soft Matter* **8**, 1673 (2012).
56. H. Yoon, H.E. Jeong, T.-i Kim, T.J. Kang, D. Tahk, K. Char, and K.Y. Suh: Adhesion hysteresis of Janus nanopillars fabricated by nanomolding and oblique metal deposition. *Nano Today* **4**, 385 (2009).
57. K.-H. Chu, R. Xiao, and E.N. Wang: Uni-directional liquid spreading on asymmetric nanostructured surfaces. *Nat. Mater.* **9**, 413 (2010).
58. C.M. Chen and S. Yang: Directed water shedding on high-aspect-ratio shape memory polymer micropillar arrays. *Adv. Mater.* **26**, 1283 (2014).
59. J.Y. Chung, J.P. Youngblood and C.M. Stafford: Anisotropic wetting on tunable micro-wrinkled surfaces. *Soft Matter* **3**, 1163 (2007).
60. P.-C. Lin and S. Yang: Mechanically switchable wetting on wrinkled elastomers with dual-scale roughness. *Soft Matter* **5**, 1011 (2009).
61. K. Khare, J. Zhou, and S. Yang: Tunable open-channel microfluidics on soft poly(dimethylsiloxane) (PDMS) substrates with sinusoidal grooves. *Langmuir* **25**, 12794 (2009).
62. A.R. Parker and C.R. Lawrence: Water capture by a desert beetle. *Nature* **414**, 33 (2001).

https://doi.org/10.1557/mrc.2015.18 Published online by Cambridge University Press

63. Y. Zheng, J. Li, E. Lee, and S. Yang: Light-induced shape recovery of deformed shape memory polymer micropillar arrays with gold nanorods. *RSC Adv.* **5**, 30495 (2015). DOI: 10.1039/c5ra01469g.
64. Z.L. Wu, R. Wei, A. Buguin, J.-M. Taulemesse, N. Le Moigne, A. Bergeret, X. Wang, and P. Keller: Stimuli-responsive topological change of microstructured surfaces and the resultant variations of wetting properties. *ACS Appl. Mater. Interfaces* **5**, 7485 (2013).
65. G. Huber, H. Mantz, R. Spolenak, K. Mecke, K. Jacobs, S.N. Gorb, and E. Arzt: Evidence for capillarity contributions to gecko adhesion from single spatula nanomechanical measurements. *Proc. Natl. Acad. Sci. U. S. A.* **102**, 16293 (2005).
66. H.E. Jeong, M.K. Kwak, and K.Y. Suh: Stretchable, adhesion-tunable dry adhesive by surface wrinkling. *Langmuir* **26**, 2223 (2010).
67. D.M. Drotlef, P. Blümler, and A. del Campo: Magnetically actuated patterns for bioinspired reversible adhesion (dry and wet). *Adv. Mater.* **26**, 775 (2014).
68. S. Reddy, E. Arzt, and A. del Campo: Bioinspired surfaces with switchable adhesion. *Adv. Mater.* **19**, 3833 (2007).
69. T. Xie and X.C. Xiao: Self-peeling reversible dry adhesive system. *Chem. Mater.* **20**, 2866 (2008).
70. R. Wang and T. Xie: Shape memory- and hydrogen bonding-based strong reversible adhesive system. *Langmuir* **26**, 2999 (2010).
71. M.G. De: *Velvet Type Fabric and Method of Producing Same* Velcro Sa Soulie, U. S. Patent No. 2,717,437 (1955).
72. Epukas: *Burdock—Arctium Tomentosum* (Wikipedia Commons, 2008).
73. A. Freeman and B. Golden: *Why didn't I Think of that: Bizarre Origins of Ingenious Inventions We Couldn't Live Without* (John Wiley & Sons, Hoboken, New Jersey, 1997).
74. C.-M. Chen, C.-L. Chiang, C.-L. Lai, T. Xie, and S. Yang: Buckling-based strong dry adhesives via interlocking. *Adv. Funct. Mater.* **23**, 3813 (2013).
75. C.R. Jin, A. Jagota, and C.Y. Hui: Structure and energetics of dislocations at micro-structured complementary interfaces govern adhesion. *Adv. Funct. Mater.* **23**, 3453 (2013).
76. H. Ko, J. Lee, B.E. Schubert, Y.L. Chueh, P.W. Leu, R.S. Fearing, and A. Javey: Hybrid core-shell nanowire forests as self-selective chemical connectors. *Nano Lett.* **9**, 2054 (2009).
77. Y. Rahmawan, S.M. Kang, S.Y. Lee, K.-Y. Suh, and S. Yang: Enhanced shear adhesion by mechanical interlocking of dual-scaled elastomeric micropillars with embedded silica particles. *Macromol. React. Eng.* **7**, 616 (2013).
78. H. Shahsavan and B.X. Zhao: Conformal adhesion enhancement on biomimetic microstructured surfaces. *Langmuir* **27**, 7732 (2011).
79. A.K. Singh, Y. Bai, N. Nadermann, A. Jagota, and C.Y. Hui: Adhesion of microchannel-based complementary surfaces. *Langmuir* **28**, 4213 (2012).
80. S. Vajpayee, K. Khare, S. Yang, C.-Y. Hui, and A. Jagota: Adhesion selectivity using rippled surfaces. *Adv. Funct. Mater.* **21**, 547 (2011).
81. C. Pang, D. Kang, T.-i Kim, and K.-Y. Suh: Analysis of preload-dependent reversible mechanical interlocking using beetle-inspired wing locking device. *Langmuir* **28**, 2181 (2011).
82. C. Pang, T.I. Kim, W.G. Bae, D. Kang, S.M. Kim, and K.Y. Suh: Bioinspired reversible interlocker using regularly arrayed high aspect-ratio polymer fibers. *Adv. Mater.* **24**, 475 (2012).
83. C. Pang, G.-Y. Lee, T.-i Kim, S.M. Kim, H.N. Kim, S.-H. Ahn, and K.-Y. Suh: A flexible and highly sensitive strain-gauge sensor using reversible interlocking of nanofibres. *Nat. Mater.* **11**, 795 (2012).
84. M. De Stefano, L. De Stefano, and R. Congestri: Functional morphology of micro- and nanostructures in two distinct diatom frustules. *Superlattices Microstruct.* **46**, 64 (2009).
85. S. Kinoshita and S. Yoshioka: Structural colors in nature: the role of regularity and irregularity in the structure. *Chem Phys Chem* **6**, 1442 (2005).
86. P. Vukusic and J.R. Sambles: Photonic structures in biology. *Nature* **424**, 852 (2003).
87. M. Srinivasarao: Nano-optics in the biological world: beetles, butterflies, birds, and moths. *Chem. Rev.* **99**, 1935 (1999).
88. Y. Takeoka: Angle-independent structural coloured amorphous arrays. *J. Mater. Chem.* **22**, 23299 (2012).
89. D.G. Stavenga, H.L. Leertouwer, N.J. Marshall, and D. Osorio: Dramatic colour changes in a bird of paradise caused by uniquely structured breast feather barbules. *Proc. R. Soc. Lond. B, Biol. Sci.* **278**, 2098 (2011).
90. A.L. Holt, A.M. Sweeney, S. Johnsen, and D.E. Morse: A highly distributed Bragg stack with unique geometry provides effective camouflage for Loliginid squid eyes. *J. R. Soc. Interface* **8**, 1386 (2011).
91. F. Liu, B.Q. Dong, X.H. Liu, Y.M. Zheng, and J. Zi: Structural color change in longhorn beetles Tmesisternus isabellae. *Opt. Express* **17**, 16183 (2009).
92. S. Zylinski and S. Johnsen: Mesopelagic cephalopods switch between transparency and pigmentation to optimize camouflage in the deep. *Curr. Biol.* **21**, 1937 (2011).
93. M. Izumi, A.M. Sweeney, D. DeMartini, J.C. Weaver, M.L. Powers, A. Tao, T.V. Silvas, R.M. Kramer, W.J. Crookes-Goodson, L. M. Mathger, R.R. Naik, R.T. Hanlon, and D.E. Morse: Changes in reflectin protein phosphorylation are associated with dynamic iridescence in squid. *J. R. Soc. Interface* **7**, 549 (2010).
94. W. Park and J.-B. Lee: Mechanically tunable photonic crystal structure. *Appl. Phys. Lett.* **85**, 4845 (2004).
95. H. Kim, J. Ge, J. Kim, S. Choi, H. Lee, W. Park, Y. Yin, and S. Kwon: Structural colour printing using a magnetically tunable and lithographically fixable photonic crystal. *Nat. Photonics* **3**, 534 (2009).
96. X. Zhu, Y. Zhang, D. Chandra, S.-C. Cheng, J.M. Kikkawa, and S. Yang: Two-dimensional photonic crystals with anisotropic unit cells imprinted from poly (dimethylsiloxane) membranes under elastic deformation. *Appl. Phys. Lett.* **93**, 161911 (2008).
97. A.C. Arsenault, T.J. Clark, G. von Freymann, L. Cademartiri, R. Sapienza, J. Bertolotti, E. Vekris, S. Wong, V. Kitaev, and I. Manners: From colour fingerprinting to the control of photoluminescence in elastic photonic crystals. *Nat. Mater.* **5**, 179 (2006).
98. D. Chandra, S. Yang, A.A. Soshinsky, and R.J. Gambogi: Biomimetic ultrathin whitening by capillary-force-induced random clustering of hydrogel micropillar arrays. *ACS Appl. Mater. Interfaces* **1**, 1698 (2009).
99. E. Lee, M. Zhang, Y. Cho, Y. Cui, J. Van der Spiegel, N. Engheta, and S. Yang: Tilted pillars on wrinkled blastomers as a reversibly tunable optical window. *Adv. Mater.* **26**, 4127 (2014).
100. C. Brennen and H. Winet: Fluid-mechanics of propulsion by cilia and flagella. *Annu. Rev. Fluid Mech.* **9**, 339 (1977).
101. U. Urutseg and L. Kohidai: *Difference of Beating Pattern of Flagellum and Cilia* (Wikipedia Commons, 2011).
102. C. Daghlian: *Scanning Electron Microscope Image of Lung Trachea Epithelium* (Wikipedia Commons, 2006).
103. P. Satir and M.A. Sleigh: The physiology of cilia and mucociliary interactions. *Annu. Rev. Physiol.* **52**, 137 (1990).
104. M.A. Sleigh, J.R. Blake, and N. Liron: The propulsion of mucus by cilia. *Am. Rev. Resp. Dis.* **137**, 726 (1988).
105. B.A. Evans, A.R. Shields, R.L. Carroll, S. Washburn, M.R. Falvo, and R. Superfine: Magnetically actuated nanorod arrays as biomimetic cilia. *Nano Lett.* **7**, 1428 (2007).
106. A. Sidorenko, T. Krupenkin, A. Taylor, P. Fratzl, and J. Aizenberg: Reversible switching of hydrogel-actuated nanostructures into complex micropatterns. *Science* **315**, 487 (2007).
107. X. He, M. Aizenberg, O. Kuksenok, L.D. Zarzar, A. Shastri, A.C. Balazs, and J. Aizenberg: Synthetic homeostatic materials with chemo-mechano-chemical self-regulation. *Nature* **487**, 214 (2012).
108. K. Autumn, Y.A. Liang, S.T. Hsieh, W. Zesch, W.P. Chan, T.W. Kenny, R. Fearing, and R.J. Full: Adhesive force of a single gecko foot-hair. *Nature* **405**, 681 (2000).

https://doi.org/10.1557/mrc.2015.18 Published online by Cambridge University Press